BIOCHEMISTRY
including biophysical chemistry & molecular biology

Article

pubs.acs.org/biochemistry

Structural Insights into the Calcium-Mediated Allosteric Transition in the C-Terminal Domain of Calmodulin from Nuclear Magnetic Resonance Measurements

Predrag Kukic,[†] Patrik Lundström,[‡] Carlo Camilloni,[†] Johan Evenäs,[§] Mikael Akke,*[,∥] and Michele Vendruscolo*[,†]

[†]Department of Chemistry, University of Cambridge, Cambridge CB2 1EW, U.K.

[‡]Department of Physics, Chemistry and Biology, Linköping University, SE-581 83 Linköping, Sweden

[§]Red Glead Discovery, Medicon Village, SE-223 81 Lund, Sweden

[∥]Department of Biophysical Chemistry, Center for Molecular Protein Science, Lund University, SE-221 00 Lund, Sweden

Supporting Information

ABSTRACT: Calmodulin is a two-domain signaling protein that becomes activated upon binding cooperatively two pairs of calcium ions, leading to large-scale conformational changes that expose its binding site. Despite significant advances in understanding the structural biology of calmodulin functions, the mechanistic details of the conformational transition between closed and open states have remained unclear. To investigate this transition, we used a combination of molecular dynamics simulations and nuclear magnetic resonance (NMR) experiments on the Ca^{2+}-saturated E140Q C-terminal domain variant. Using chemical shift restraints in replica-averaged metadynamics simulations, we obtained a high-resolution structural ensemble consisting of two conformational states and validated such an ensemble against three independent experimental data sets, namely, interproton nuclear Overhauser enhancements, ^{15}N order parameters, and chemical shift differences between the exchanging states. Through a detailed analysis of this structural ensemble and of the corresponding statistical weights, we characterized a calcium-mediated conformational transition whereby the coordination of Ca^{2+} by just one oxygen of the bidentate ligand E140 triggers a concerted movement of the two EF-hands that exposes the target binding site. This analysis provides atomistic insights into a possible Ca^{2+}-mediated activation mechanism of calmodulin that cannot be achieved from static structures alone or from ensemble NMR measurements of the transition between conformations.

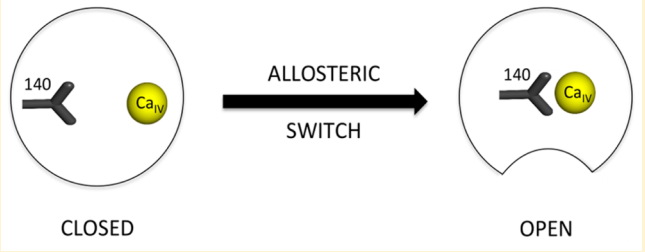

Calcium ions (Ca^{2+}) serve as second messengers in a wide range of cellular processes, including cell cycle control, cell differentiation, nucleotide metabolism, muscle contraction, and signal transduction.[1,2] The Ca^{2+} messenger system includes proteins fine-tuned for a rapid response to transient variations in the intracellular Ca^{2+} concentration. A remarkable feature of these proteins is the extent of structural similarity of their Ca^{2+} binding units, which are mainly composed of the highly homologous helix−loop−helix motif, the so-called "EF-hand", which generally appears in coupled pairs that show positive cooperativity with respect to Ca^{2+} binding.

The conformational response to Ca^{2+} binding differs markedly among EF-hand proteins.[3,4] While Ca^{2+} binding to EF-hand proteins involved in Ca^{2+} buffering and transport typically causes only very small structural changes, as in the case of calbindin D_{9k},[5−7] Ca^{2+} binding to EF-hand proteins active in regulation often induces substantial structural changes, as in the case of calmodulin (CaM)[8−10] and skeletal troponin C (TnC).[11] Both CaM and skeletal TnC switch upon Ca^{2+} binding from closed to open structures with exposed hydrophobic patches capable of binding target proteins. Even though the end states of the conformational switch in CaM and skeletal TnC have been described in detail,[3,9−16] the corresponding allosteric mechanism is still not fully understood, in particular in terms of the detailed relationship among Ca^{2+} coordination, local interactions within the Ca^{2+} binding loops, and concerted movements of the α-helices in the EF-hand pairs, which are required to form the binding site.

To clarify the allosteric mechanism of the conformational transition in CaM, we consider here the E140Q mutational variant of the C-terminal domain of CaM (E140Q-TR_2C) for which extensive experimental studies have been reported.[17−19] The notation TR_2C originates from early work using tryptic fragments of CaM,[16,20] where TR_1C and TR_2C denote the N- and C-terminal fragments, respectively. TR_2C refers here to the isolated C-terminal domain, comprising residues 76−148, while cCaM refers to the same segment in the context of full-length

Received: August 30, 2015
Revised: November 26, 2015
Published: November 30, 2015

DOI: 10.1021/acs.biochem.5b00961
Biochemistry 2016, 55, 19−28

CaM. The TR_2C construct with the wild-type sequence (WT-TR_2C) has been studied extensively in the past[16,20] because it retains the Ca^{2+} binding properties observed for cCaM and provides a means of reducing the complexity of the system. WT-TR_2C consists of a pair of EF-hands, whose α-helices are almost antiparallel in the apo (Ca^{2+}-free) state and rearrange into a perpendicular orientation in the holo (Ca^{2+}-saturated) state (Figure S1). These structural changes upon Ca^{2+} binding mirror those observed for cCaM,[9,16] further validating TR_2C as an adequate model system for cCaM. TR_2C binds one Ca^{2+} to each of the two EF-hands with high affinity ($K_d \sim 10^{-6}$ M) and strong positive cooperativity between the sites.[20]

To circumvent the positive cooperativity of Ca^{2+} binding, and to gain more insight into the activation of CaM by Ca^{2+} ions, the E104Q and E140Q variants of TR_2C have been studied in the past.[17−19] The E140Q variant targets the bidentate Ca^{2+}-ligating carboxylate group in loop IV, forcing the Ca^{2+} coordination by residue 140 to be monodentate (Figure S2); similarly, E104Q affects the corresponding residue in loop III. As a result, the affinity for Ca^{2+} of loop IV (or III) is drastically reduced, allowing the observation of the intermediate state with only one Ca^{2+} bound.[15] Furthermore, in the Ca^{2+}-saturated state, these variants undergo exchange dynamics between open and closed conformers.[18,19,21,22] Therefore, they present an opportunity to explore the relationships between the conformational changes and Ca^{2+} coordination that underlie the allosteric switch in EF-hand pairs. Here we use E140Q-TR_2C as a model system to investigate this issue in great detail.

E140Q-TR_2C is a powerful model system, because the E140Q mutation causes only minor perturbations in the structure of the apo state, as observed from the close correspondence of the $^1H-^{15}N$ HSQC spectra of apo-WT-TR_2C and apo-E140Q-TR_2C.[17] By contrast, the chemical shifts of the Ca^{2+}-saturated states show that there are major differences between the conformational ensembles of the wild-type and mutant proteins in their holo forms. Previous NMR studies have shown that the Ca^{2+}-saturated state of E140Q-TR_2C, denoted here as $(Ca^{2+})_2$-E140Q-TR_2C, exchanges between at least two conformations on the submillisecond time scale.[19,21,22] These two conformations were suggested to be similar to the closed (apo) and open (holo) states of WT-TR_2C, as gauged from two mutually exclusive sets of interproton distances in the NOESY spectra of $(Ca^{2+})_2$-E140Q-TR_2C.[17] The structural transition between the two states in $(Ca^{2+})_2$-E140Q-TR_2C has also been addressed in the past using heteronuclear relaxation experiments[18,19] and has been shown to be similar to the exchange between the open and closed states in apo-WT-TR_2C.[23] Both the NOESY and relaxation experiments suggest that the two dominant conformational states of $(Ca^{2+})_2$-E140Q-TR_2C have approximately equal populations. Thus, this system offers unique opportunities to investigate the mechanism of transition between closed and open states in cCaM. However, a high-resolution structural analysis has not previously been possible because of methodological challenges in interpreting the experimental data in terms of conformational ensembles.

In this study, we provide a detailed view of the conformational transition between the closed and open states of cCaM, based on NMR chemical shifts measured for $(Ca^{2+})_2$-E140Q-TR_2C. We use the chemical shift information within the replica-averaged metadynamics (RAM) method,[24] in which bias-exchange metadynamics is combined with a chemical shift-based penalty function implemented in the force field.[25−28] The resulting ensemble of conformations exhibits two basins in the free energy landscape of $(Ca^{2+})_2$-E140Q-TR_2C, corresponding to two subensembles that resemble the apo and holo states of the C-terminal domain of CaM. We validate these subensembles against three independent experimental data sets, namely, chemical shift differences determined by ^{15}N $R_{1\rho}$ relaxation dispersion experiments, $^1H-^1H$ NOE connectivities, and ^{15}N order parameters, all of which show very good agreement with the corresponding parameters back-calculated from the ensembles. The conformational ensembles that we describe here provide a high-resolution structural characterization of the $(Ca^{2+})_2$-E140Q-TR_2C state and offer unprecedented details about the trigger point underlying the conformational transition of the EF-hands in cCaM.

MATERIALS AND METHODS

Sample Preparation. The uniformly ^{13}C- and ^{15}N-enriched E140Q variant of TR_2C was obtained by overexpression in *Escherichia coli* BL21(DE3) cells using M9 medium supplemented with [^{13}C]glucose and $^{15}NH_4Cl$ as the sole carbon and nitrogen sources, respectively. The NMR sample consisted of ^{13}C- and ^{15}N-labeled E140Q (0.7 mM) supplemented with $CaCl_2$ (20 mM), 2,2-dimethyl-2-silapentane-5-sulfonic acid (DSS; 100 μM), and NaN_3 (200 μM) in 10% D_2O at pH 6.0. Under these conditions, the calcium-saturated state is populated to >98%.[17]

NMR Spectroscopy. NMR data were acquired at 35 °C using Varian INOVA (600 MHz) NMR spectrometers equipped with triple-resonance probes with pulsed-field gradients. ^{15}N and ^1H assignments of $(Ca^{2+})_2$-E140Q-TR_2C have been reported previously.[17] For the purpose of this study, we recorded triple-resonance heteronuclear NMR spectra of $(Ca^{2+})_2$-E140Q-TR_2C [HNCO, HNCA, HN(CO)CA, HN(CA)CB, and HN(COCA)CB] and conducted complete assignments of the backbone ^1H, ^{15}N, and ^{13}C, as well as the $^{13}C^{\beta}$ nuclei, to obtain a comprehensive set of chemical shifts for use as restraints in the RAM simulations. Distance constraints were obtained through the analysis of heteronuclear three-dimensional (3D) NOESY spectra. These were 3D $^1H-^{15}N$ and 3D $^1H-^{13}C$ NOESY-HSQC spectra with mixing times of 150 ms for the $^1H-^{15}N$ and $^1H-^{13}C^{aliphatic}$ detected experiments and 100 ms for the $^1H-^{13}C^{aromatic}$ detected experiments. The experimental protocols included the use of pulsed-field gradients for coherence order selection[29] and in the case of the $^1H-^{15}N$ detected experiments for sensitivity enhancement.[30]

$R_{1\rho}$ Relaxation Dispersion Measurements. ^{15}N off-resonance rotating-frame relaxation experiments were conducted here, as described in ref 19, yielding rate constants, $R_{1\rho}$, within the errors of previous measurements,[19,22] thus validating the previous results. For a two-state exchange process between the open and closed conformations, the exchange contribution in the fast-exchange limit ($|\tau_{ex}\Delta\omega| \ll 1$) is given by

$$R_{ex} = \phi\tau_{ex}/(1 + \tau_{ex}^2\omega_e^2) \quad (1)$$

with

$$\phi = p_o p_c \Delta\omega^2 \quad (2)$$

where τ_{ex} is the mean lifetime, ω_e is the strength of the radiofrequency spin-lock field, p_o and p_c are the populations of the open and closed states, respectively, and $\Delta\omega = \gamma_{N/H}B_0\Delta\delta_{N/H}$, where $\gamma_{N/H}$ is the gyromagnetic ratio of ^{15}N or ^1H, B_0 is the strength of the static magnetic field, and $\Delta\delta$ is the

DOI: 10.1021/acs.biochem.5b00961
Biochemistry 2016, 55, 19−28

chemical shift difference (in parts per million) between the two states. The conformational exchange of the backbone amide groups was characterized by optimizing the parameters τ_{ex} and ϕ simultaneously against the measured ^{15}N and previously reported $^{1}H^{N}$[19,22] $R_{1\rho}$ data sets. Both τ_{ex} and ϕ were optimized in a residue-specific manner. However, very similar values of ϕ resulted when τ_{ex} was optimized globally.

RAM Simulations. The RAM simulations were performed using GROMACS[31] interfaced with PLUMED[32] and Almost,[33] as described in ref 26. The Amber99SB-ILDN force field[34] with the TIP3P water model[35] was modified using a chemical shift-based energy term defined as

$$E_{CS} = \sum_{i=76}^{148} \sum_{j=1}^{6} E_{ij}(\delta_{ij}^{calc} - \delta_{ij}^{exp}) \quad (3)$$

where E_{ij} is a chemical shift-based energy term that corresponds to an atom of type j (H^{α}, H^{N}, N, C^{α}, C^{β}, or C′) and to the ith residue of $(Ca^{2+})_2$-E140Q-TR$_2$C. The experimental chemical shifts δ_{ij}^{exp} of $(Ca^{2+})_2$-E140Q-TR$_2$C residues were measured in this study. Their corresponding calculated values, δ_{ij}^{calc}, were obtained as averages over four replicas.[26]

The starting conformation was taken from a crystallographically obtained structure [Protein Data Bank (PDB) entry 1CLL[14]] (residues 76−148 and the E to Q mutation at position 140) with two Ca^{2+} ions coordinated by loops III and IV. The structure was initially solvated in a water box extending 12 Å from its surface and then energy minimized. All simulations were conducted in the canonical ensemble by keeping the volume fixed and by thermostating the system with the modified Berendsen thermostat at 300 K. The net charge was neutralized by adding nine Na^{+} ions. The system was evolved with a time step of 2 fs by constraining the fast-bonded modes using LINCS.[31] We accounted for van der Waals interactions by using a cutoff of 12 Å. The particle mesh Ewald method[36] with a grid spacing of 1.09 Å was used for the electrostatic contribution to nonbonded interactions. The two Ca^{2+} ions stayed in loops III and IV during the course of the simulation without any need to restrain them.

The inclusion of replica-averaged chemical shifts into the force field generated an ensemble of $(Ca^{2+})_2$-E140Q-TR$_2$C conformations compatible with the given set of NMR chemical shifts in the sense of the maximum entropy principle.[37,38]

Collective Variables. The simulation was performed using four replicas, one for each of the CVs.

(1) CV1 (dihedral correlation) acts on 72 ϕ and ψ dihedral angles of all residues in the protein (parameters, Gaussian width σ of 0.1). (2) CV2 (dihedral correlation) acts on 17 χ_1 angles that belong to all heavy side-chain residues (Phe, His, Tyr, Trp, Arg, Lys, and Met) (parameters, Gaussian width σ of 0.1). (3) CV3 (angle) acts on the interhelical angle of the third EF-hand. The angle is defined by the center of mass of three groups of C_{α} atoms: α-helix E (residues 83−91), loop III (residues 93−100), and α-helix F (residues 102−111) (parameters, Gaussian width σ of 0.05). (4) CV4 (angle) acts on the interhelical angle of the fourth EF-hand. This angle is defined by the center of mass of three groups of C^{α} atoms: α-helix G (residues 118−127), loop IV (residues 129−136), and α-helix H (residues 139−145) (parameters, Gaussian width σ of 0.05).

Free Energy Reconstruction in the CV Space. The bias potentials became stable after a simulation time t_{eq} of ∼150 ns. The simulation was further run for an additional 80 ns to reconstruct the free energy landscape of the protein. The free energy of each microstate was estimated by a WHAM approach as described previously[39] using the METAGUI[40] and Visual Molecular Dynamics[41] interface. In total, 2840 microstates were identified, and their free energy values were computed according to the corresponding bias potentials and the populations observed after t_{eq}.

According to the interhelical angles (CV1 and CV2), the microstates were clustered into two groups representing openlike and closedlike ensembles. The two Ca^{2+} ions were present in loops III and IV in both ensembles. Their ligands (Figure S2) present at the start of the simulation remained in the coordination sphere in both ensembles (see Discussion). Water molecules did not stay in the binding pocket for more than 10 ns. In the low-free energy openlike conformation, Ca^{2+} is ∼0.3 Å from starting structure 1CLL and the E140Q mutation does not seem to change the way Ca^{2+} sits in the binding pocket. The same applies to loop IV in the open conformation, which adopts a conformation very close to that of 1CLL [root-mean-square deviation (rmsd) of 0.9 Å].

RESULTS

Bimodal Conformational Ensemble of $(Ca^{2+})_2$-E140Q-TR$_2$C. We implemented replica-averaged chemical shift restraints in RAM simulations to determine an ensemble of conformations representing the conformational fluctuations of $(Ca^{2+})_2$-E140Q-TR$_2$C. First, we recorded triple-resonance heteronuclear NMR spectra of $(Ca^{2+})_2$-E140Q-TR$_2$C and conducted complete assignments of the backbone ^{1}H, ^{15}N, and ^{13}C, as well as the $^{13}C^{\beta}$ nuclei, to obtain a comprehensive set of chemical shifts for use as restraints. The differences between the $^{1}H^{N}$, ^{15}N, $^{13}C^{\alpha}$, and $^{13}C^{\beta}$ chemical shifts of $(Ca^{2+})_2$-E140Q-TR$_2$C and the corresponding shifts of $(Ca^{2+})_2$-cCaM[42] are shown in Figure S3. These chemical shift assignments extend and confirm previous results,[17] showing that many backbone chemical shifts of the Ca^{2+}-saturated states of the wild type and E140Q variants are quite different, in stark contrast to those of the apo forms.[17] Notably, these differences are distributed across both EF-hands, indicating that the E140Q mutation has significant effects on the $(Ca^{2+})_2$-bound state of TR$_2$C. Moreover, the backbone chemical shifts of $(Ca^{2+})_2$-E140Q-TR$_2$C have values that are between the values of the apo and holo states of cCaM, thus corroborating the concept that $(Ca^{2+})_2$-E140Q-TR$_2$C populates a mixture of conformations similar to the apo and holo states of cCaM.[18,19,23]

As an initial investigation of the structural differences between $(Ca^{2+})_2$-E140Q-TR$_2$C and $(Ca^{2+})_2$-cCaM, we determined their secondary structure populations from the measured chemical shifts using the δ2D method[43] (Figure S4). For the majority of residues, the obtained differences are not statistically significant. Some differences are detected for the second β-strand, which likely originate from the mutation of E140, whose side-chain oxygen atom forms a hydrogen bond with the backbone of this β-strand in $(Ca^{2+})_2$-cCaM. Overall, however, $(Ca^{2+})_2$-E140Q-TR$_2$C retains the secondary structure of $(Ca^{2+})_2$-cCaM.

We then used the backbone and $^{13}C^{\beta}$ chemical shifts of $(Ca^{2+})_2$-E140Q-TR$_2$C as replica-averaged chemical shift restraints in the RAM simulations to determine an ensemble of conformations representing the structural heterogeneity of this state. The RAM approach provides an accurate approximation of the Boltzmann distribution of $(Ca^{2+})_2$-E140Q-TR$_2$C in which the restraints are implemented in a replica-averaged manner according to the maximum entropy principle,[37,38] and

DOI: 10.1021/acs.biochem.5b00961
Biochemistry 2016, 55, 19−28

the sampling is conducted by metadynamics (see Materials and Methods). In the latter, a time-dependent potential is used that discourages the exploration of already visited regions of the conformational space described in terms of specific functions of the atomic coordinates, i.e., collective variables (CVs). Four CVs were employed here. Two CVs act on the tertiary structure of the $(Ca^{2+})_2$-E140Q-TR_2C state by biasing the sampling of the backbone ϕ and ψ dihedral angles, as well as the χ_1 angles of residues with heavy side chains. Another two CVs act on the interhelical angles of the two EF-hands, to sample a wider range of helical orientations.

The resulting $(Ca^{2+})_2$-E140Q-TR_2C ensemble is shown in Figure 1 as a function of interhelical angles between the first and second EF-hands and exhibits a bimodal distribution of conformations. In contrast, a control simulation in which the RAM protocol was applied to $(Ca^{2+})_2$-cCaM shows mainly the presence of typical open (holo) conformations (Figure S5). The two groups of conformations in the $(Ca^{2+})_2$-E140Q-TR_2C ensemble are further related in Figure 1 to the corresponding interhelical angles extracted from the deposited PDB[44] structures of the closed apo-WT-TR_2C (gray, PDB entry 1CMF[16]) and open $(Ca^{2+})_2$-cCaM (blue, PDB entries 1CLL,[14] 3CLN,[13] 1UP5,[45] and 4BW8[46]). The lowest free energy minimum of $(Ca^{2+})_2$-E140Q-TR_2C includes conformations with interhelical angles closer to those of $(Ca^{2+})_2$-cCaM. By contrast, the slightly higher free energy minimum includes configurations with interhelical angles closer to those of apo-WT-TR_2C. The free energy difference between these two conformational basins is 0.2 kJ/mol, which is well within the error (≈2 kJ/mol) of the weighted-histogram analysis method (WHAM)[39] that we used to calculate the free energy. Therefore, the populations of the two groups of conformations are very similar (p_c = 48 ± 6%, and p_o = 52 ± 6%), a result fully consistent with the equal populations previously estimated from independent relaxation dispersion measurements of the $(Ca^{2+})_2$-E140Q-TR_2C state.[19]

The similarities of the two conformational ensembles of $(Ca^{2+})_2$-E140Q-TR_2C to apo-WT-TR_2C and Ca^{2+}-cCaM were further quantified by calculating their root-mean-square (rms) distances to apo-WT-TR_2C and Ca^{2+}-cCaM structures extracted from the PDB (Figure 2). The conformations with more open EF-hands have an average rmsd from the $(Ca^{2+})_2$-cCaM structures (⟨rmsd⟩ = 2.7 Å) significantly lower than that from the apo-WT-TR_2C structures (⟨rmsd⟩ = 5.2 Å). However, the interhelical angles in these open conformations are still smaller than those in the $(Ca^{2+})_2$-cCaM ensemble, possibly because of the lack of one Ca^{2+} coordinating oxygen in loop IV. The conformations with more closed EF-hands have rmsd values from the apo-WT-TR_2C ensemble (⟨rmsd⟩ = 3.9 Å) only slightly lower than those from the $(Ca^{2+})_2$-cCaM ensemble (⟨rmsd⟩ = 4.3 Å). The relatively high rmsd values of these structures from apo-WT-TR_2C are caused primarily by differences in the conformations of loops III and IV, rather than the rest of the protein (Figure 2b). These results are expected because loops III and IV coordinate two Ca^{2+} atoms

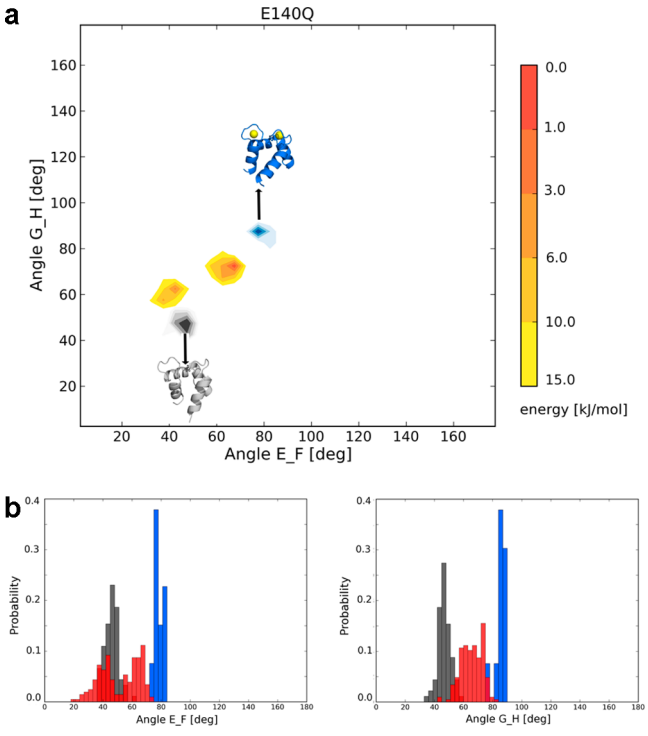

Figure 1. Free energy landscape of $(Ca^{2+})_2$-E140Q-TR_2C as a function of the angles between α-helices E and F (angle E_F) and α-helices G and H (angle G_H). (a) Two free energy minima are detected: the first in proximity of a previously determined apo-WT-TR_2C structure (gray, PDB entry 1CMF) and the second near a series of known $(Ca^{2+})_2$-cCaM structures (blue, PDB entries 1CLL, 3CLN, 1UP5, and 4BW8). (b) Comparison between the distributions of the E_F and G_H angles from the $(Ca^{2+})_2$-E140Q-TR_2C ensemble (red) and the corresponding distributions of the structures of apo-WT-TR_2C (gray) and $(Ca^{2+})_2$-cCaM (blue).

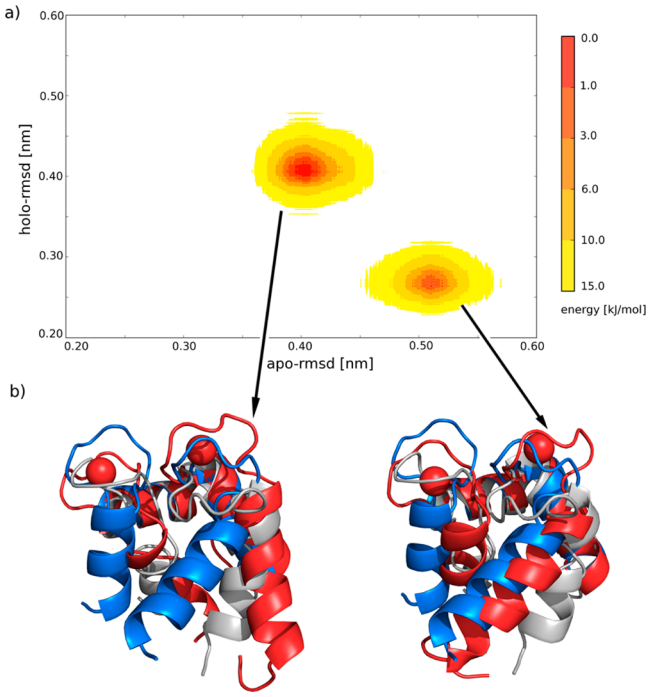

Figure 2. (a) Free energy landscape of $(Ca^{2+})_2$-E140Q-TR_2C as a function of the rms distance from the representative structures of apo-WT-TR_2C (PDB entry 1CMF) and $(Ca^{2+})_2$-cCaM (PDB entries 1CLL, 3CLN, 1UP5, and 4BW8); rms distances are calculated using all heavy atoms. (b) Two representative structures (red) of the two free energy minima superimposed onto apo-WT-TR_2C (gray, PDB entry 1CMF, model 1) and $(Ca^{2+})_2$-cCaM (blue, PDB entry 1CLL) using α-helices F and G.

DOI: 10.1021/acs.biochem.5b00961
Biochemistry 2016, 55, 19−28

in $(Ca^{2+})_2$-E140Q-TR_2C, while the binding sites are empty and highly flexible in apo-WT-TR_2C.[8]

Validation of the Bimodal Conformational Ensemble of $(Ca^{2+})_2$-E140Q-TR_2C. We validated the bimodal ensemble of $(Ca^{2+})_2$-E140Q-TR_2C with three distinct sets of experimental data that were all determined in a manner independent of the chemical shifts used to restrain the RAM simulations. These three data sets are distance restraints, determined from NOE connectivities; chemical shift differences between the two exchanging states, determined from ^{15}N and ^{1}H rotating-frame relaxation dispersion experiments; and ^{15}N order parameters, determined from ^{15}N laboratory-frame relaxation experiments.

First, we determined $^{1}H-^{1}H$ NOE connectivities characteristic of short distances by recording ^{15}N NOESY-HSQC[29,30] and aliphatic (ali) as well as aromatic (aro) ^{13}C NOESY-HSQC spectra.[29] Manual assignment of NOE cross-peaks resulted in 828 unambiguous, nonsequential inter-residue connectivities, partitioned as 240 $H^{N}H$, 511 $H^{ali}H$, and 77 $H^{aro}H$. These connectivities significantly extend the NOE data set presented previously.[17] The resulting experimental restraints were then compared to the corresponding interproton distances in four ensembles: the apo-WT-TR_2C and the $(Ca^{2+})_2$-cCaM ensembles extracted from the PDB, the combination of these two ensembles, and the ensemble of the $(Ca^{2+})_2$-E140Q-TR_2C structures generated in this study. A restraint was considered violated if the ensemble did not include any conformations in which the corresponding distance was <5 Å. The numbers of violated NOEs for each ensemble are listed in Table 1.

Table 1. Numbers of Violated NOE Restraints (d_{HH} > 5 Å across the ensemble) Obtained from ^{15}N NOESY-HSQC and ^{13}C NOESY-HSQC Spectra of $(Ca^{2+})_2$-E140Q-TR_2C[a]

	no. of NOE violations			
ensemble	$H^{N}H$ (240)	$H^{ali}H$ (511)	$H^{aro}H$ (77)	total (828)
apo-cCaM	51	108	26	185
$(Ca^{2+})_2$-cCaM	28	83	16	127
apo-cCaM and $(Ca^{2+})_2$-cCaM	1	9	5	15
$(Ca^{2+})_2$-E140Q-Tr_2C	0	2[b]	1[c]	3

[a]The total number of inter-residue nonsequential NOE restraints is given in parentheses. [b]R106 Hd−I125 Hd1, F92 Hz−E104 Ha. [c]F92 Hz−F141 Hd.

The full set of NOE restraints is not fulfilled by either of the apo-WT-TR_2C or $(Ca^{2+})_2$-cCaM PDB structure ensembles, as evidenced by the relatively large number of restraint violations, viz., 185 or 127, respectively (Table 1). By stark contrast, the chemical shift-derived $(Ca^{2+})_2$-E140Q-TR_2C ensemble shows very good agreement with the experimental NOE restraints, which are violated in only three cases. Similar results were obtained when the apo-WT-TR_2C and $(Ca^{2+})_2$-CaM ensembles were merged, resulting in 15 violations. These findings strongly corroborate the proposal that $(Ca^{2+})_2$-E140Q-TR_2C includes two states in fast exchange on the NMR chemical shift time scale that are similar to apo-WT-TR_2C and $(Ca^{2+})_2$-cCaM.[17] The three remaining violations arise because of local conformational deviations of the RAM-derived ensemble, resulting from remaining imprecision in the chemical shift-based bias. The violation of the R106 Hd−I125 Hd1 connectivity is likely caused by imprecision in the rotameric states of R106 and/or I125, whereas F92 Hz−E104 Ha and F92 Hz−F141 Hd connectivities most probably include imprecision in the F92 ring conformation in the apo-like state. The number of violations of the chemical shift-derived $(Ca^{2+})_2$-E140Q-TR_2C ensemble was by far the lowest among the values of the four ensembles, and all three violations showed errors that were on average <1.0 Å. These results suggest that the two conformational states determined by the chemical shift-restrained RAM approach constitute very good models of the exchanging $(Ca^{2+})_2$-E140Q-TR_2C conformers, with a high level of accuracy. Furthermore, our results highlight the similarities of these states to the apo-WT-TR_2C and $(Ca^{2+})_2$-cCaM structures.

Second, we also validated the RAM ensemble against the so-called ϕ values ($\phi = p_A p_B \Delta\omega^2$, where p_i denotes the relative population of state i and $\Delta\omega$ is the chemical shift difference between the two states), determined from amide ^{15}N and ^{1}H off-resonance $R_{1\rho}$ relaxation dispersion data measured anew on $(Ca^{2+})_2$-E140Q-TR_2C, as described previously[19,22] (see Materials and Methods). The $R_{1\rho}$ relaxation dispersion measurements suggest that two states exchange fast on the NMR chemical shift time scale: the mean lifetime (τ_{ex}) was ≈20 μs, so that $|\tau_{ex}\Delta\omega| \ll 1$ for all residues.[19,22] Thus, the determined ϕ values contain information about both the populations of the exchanging states and the differences between their chemical shifts (eq 2). Assuming equal populations of the two states, the ϕ values yield the chemical shift differences between the exchanging states as $|\Delta\delta_N| = |2\phi_N^{0.5}/\gamma_N B_0|$ and $|\Delta\delta_H| = |2\phi_H^{0.5}/\gamma_H B_0|$.

In total, the data set consisted of 57 $|\Delta\delta_N|$ and 32 $|\Delta\delta_H|$ values, which we first compared to the differences between the experimentally measured chemical shifts of the apo-WT-TR_2C and $(Ca^{2+})_2$-cCaM states (Figure 3a,b). The resulting rmsds were as follows: $rmsd_N$ = 1.8 ppm, and $rmsd_H$ = 0.40 ppm. These relatively low rmsd values are consistent with the proposal that the observed exchange involves two conformations similar to apo-WT-TR_2C and $(Ca^{2+})_2$-cCaM.[17] We then compared the $|\Delta\delta_N|$ and $|\Delta\delta_H|$ values to the predicted chemical shift differences, obtained using the CamShift method,[47] of the two states from the chemical shift-derived $(Ca^{2+})_2$-E140Q-TR_2C ensemble (Figure 3e,f). In this case, the rmsds were even lower ($rmsd_N$ = 0.90 ppm, and $rmsd_H$ = 0.20 ppm) than the corresponding values obtained for the comparison with the experiments and once more confirmed the accuracy of the chemical shift-derived $(Ca^{2+})_2$-E140Q-TR_2C ensemble. Further, we also compared the $|\Delta\delta_N|$ and $|\Delta\delta_H|$ values to CamShift-predicted chemical shift differences between the apo-WT-TR_2C and $(Ca^{2+})_2$-cCaM ensembles from the PDB (Figure 3c,d). The resulting differences were worse than those obtained from the experimental data ($rmsd_N$ = 2.78 ppm, and $rmsd_H$ = 0.43 ppm), a result that is probably caused by the inaccuracy of chemical shift predictors that can have considerable influence on $\Delta\delta$ values, as opposed to the good correlation obtained from the experimentally measured values (see Figure 3 of ref 19).

Third, we further validated the ensemble against S^2 order parameters. Unlike the ϕ values and NOE restraints, which reflect conformational changes due to the slow (microsecond to millisecond) time-scale exchange between the two basins of $(Ca^{2+})_2$-E140Q-TR_2C, the S^2 order parameters probe the motions on the picosecond to nanosecond time scale, i.e., the structural fluctuations within the individual conformational basins. Specifically, the S^2 order parameters previously measured by Evenäs et al.[18] were used here for the purpose of validation. S^2 values were predicted initially for each of the

DOI: 10.1021/acs.biochem.5b00961
Biochemistry 2016, 55, 19−28

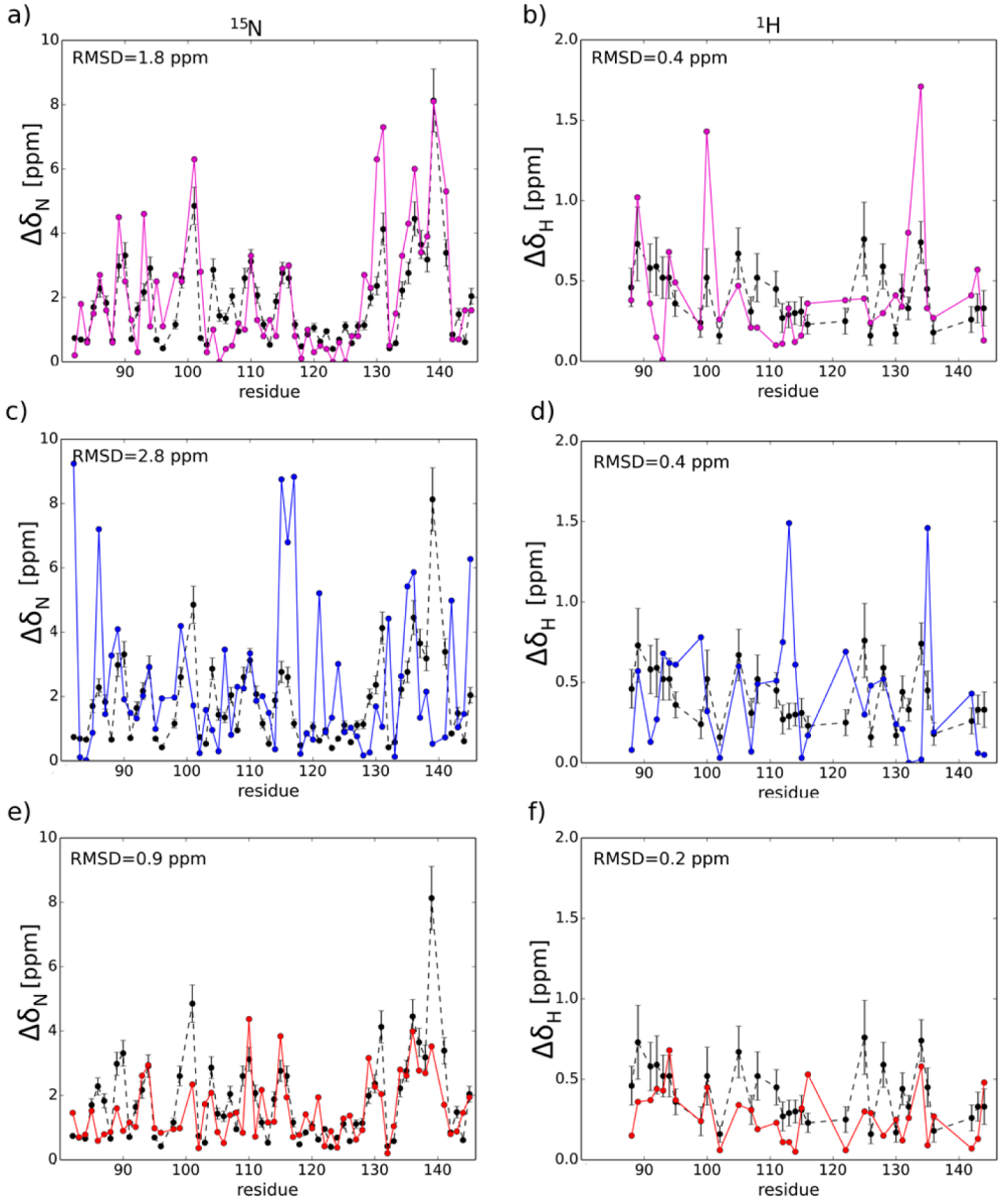

Figure 3. Comparison between the experimentally determined chemical shift difference between the exchanging states, $|2\phi^{1/2}/(\gamma_{N/H}B_0)|$, and the difference in chemical shifts of two states, as determined from (a and b) experimentally measured chemical shifts of apo-WT-TR_2C and $(Ca^{2+})_2$-cCaM, (c and d) predicted chemical shifts based on the apo-WT-TR_2C and $(Ca^{2+})_2$-cCaM ensembles, and (e and f) predicted chemical shifts for the two states identified in the chemical shift-derived $(Ca^{2+})_2$-E140Q-TR_2C ensemble.

two individual chemical shift-derived states $(Ca^{2+})_2$-E140Q-TR_2C and then averaged (Figure 4). The results obtained suggest relatively small fluctuations within the individual states and are consistent with the relatively high S^2 order parameters measured for $(Ca^{2+})_2$-E140Q-TR_2C.[18] High order parameters are present in both loop III and loop IV, as well as in all four α-helices, while the lowest S^2 values were observed for the linker that connects the two EF-hands. The predicted S^2 values gave a relatively low Q factor of 0.1 to the experimental measurements, indicating that the bimodal chemical shift-derived ensemble correctly reflects the fast time-scale fluctuations within each of the two states.

DISCUSSION

The detailed analysis of the structural ensemble of $(Ca^{2+})_2$-E140Q-TR_2C that we have reported is relevant for improving our understanding of the Ca^{2+}-induced conformational change of CaM, as suggested by previous NMR studies of apo-CaM[10,48] and apo-WT-TR_2C,[23] which revealed a population of an open conformation of approximately 5−10%. The exchange contributions to the transverse relaxation rates of apo-WT-TR_2C and $(Ca^{2+})_2$-E140Q-TR_2C have been found to be highly correlated, with an r_c of 0.86,[23] suggesting that apo-WT-TR_2C and $(Ca^{2+})_2$-E140Q-TR_2C exhibit a common conformational-exchange process.[19,23] Thus, it appears the conformation of cCaM is inherently bistable. To circumvent the positive cooperativity of Ca^{2+} binding and to gain more insight into the activation of cCaM by Ca^{2+} ions, the E140Q variants of TR_2C have been studied here. The E140Q variant targets the bidentate Ca^{2+}-ligating carboxylate group in loop IV, forcing the Ca^{2+} coordination by residue 140 to be monodentate.[17−19] In the Ca^{2+}-saturated state, this variant undergoes exchange

DOI: 10.1021/acs.biochem.5b00961
Biochemistry 2016, 55, 19−28

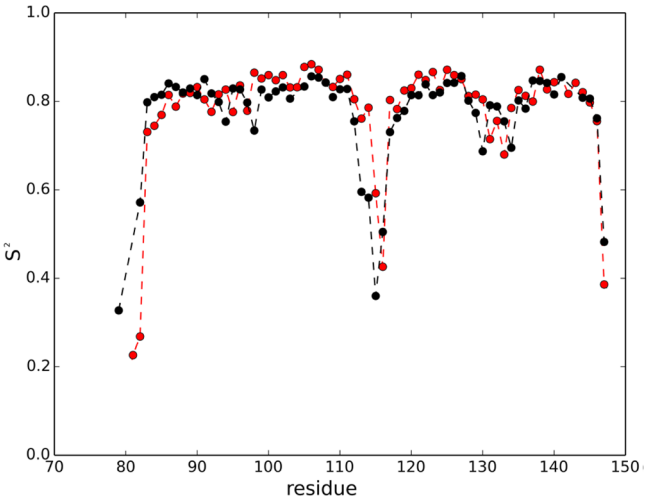

Figure 4. Comparison between experimentally determined S^2 order parameters (black) and values predicted from the $(Ca^{2+})_2$-E140Q-TR_2C ensemble.

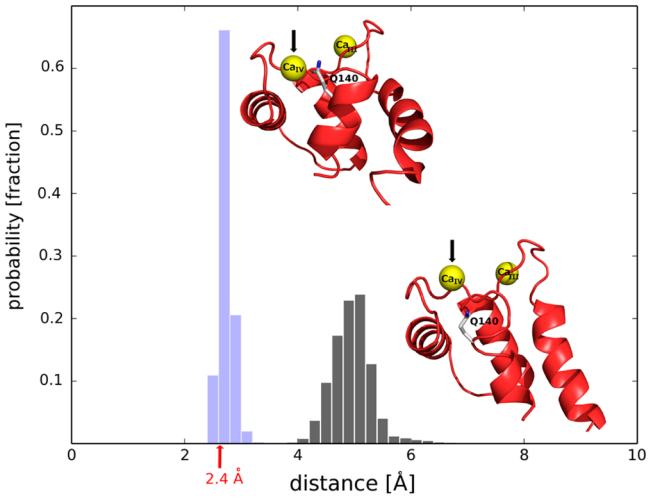

Figure 5. Distance distribution between the Q140 side-chain oxygen and Ca^{2+} ion bound in loop IV in the $(Ca^{2+})_2$-E140Q-TR_2C ensemble. The distribution is bimodal and coincides with the holo-like (blue) and apo-like (gray) subensembles. The average distance between the E140 side chain oxygen atoms and the calcium ion in EF-hand proteins is indicated by a red arrow at 2.4 Å.

dynamics between open and closed conformers.[18,19,21,22] Because the populations between the openlike and closedlike states are nearly equal in the $(Ca^{2+})_2$-E140Q-TR_2C state, this variant represents a suitable model system for probing in detail the structural transition in WT-TR_2C and CaM in general.

To obtain insights into the Ca^{2+}-induced conformational transition in CaM, we compared structural details of the closed, apo-like and open, holo-like conformations in the $(Ca^{2+})_2$-E140Q-TR_2C ensemble. This analysis has provided a detailed picture of the relationships among (i) Ca^{2+} coordination in loop IV, (ii) local conformational changes within the loops, and (iii) the large-scale structural rearrangements in the hydrophobic core that expose the consensus binding site for target proteins.

(i) A comparison of the Ca^{2+} coordination in loop IV in the two subensembles reveals an important structural feature: the side-chain oxygen of the mutated Q140 residue is in the correct geometry for Ca^{2+} coordination in all conformers of the holo-like subensemble, but not in a single conformer of the apo-like subensemble (Figure 5). The distance distribution between the side-chain oxygen of Q140 and the Ca^{2+} ion in loop IV is very narrow in the holo-like conformations with an average value of 2.5 Å (Figure 5, blue distribution). An almost identical average distance between the carboxylate oxygen of E140 and the Ca^{2+} ion in loop IV is found in the holo state of CaM structures deposited in the PDB.[49] By contrast, the side-chain oxygen of Q140 in the apo-like conformations of $(Ca^{2+})_2$-E140Q-TR_2C does not coordinate the Ca^{2+} ion in loop IV and has an average distance of 5.2 Å from the Ca^{2+} ion (Figure 5, gray distribution). This reorientation of the Q140 side chain is further associated with changes in the hydrogen bonding network and backbone torsion angles that lead to distinct conformational changes of the protein core, as described in the following.

(ii) The differences in the hydrogen bonding network and torsion angles between the two states are pronounced in loop IV (Table S1 and Figure S6f). The side chain of the first residue in loop IV, D129, is hydrogen bonded to the sixth residue of the same loop, G134, in all conformers of the holo-like ensemble, but not in a single conformer of the apo-like ensemble. The same hydrogen bond between the first and sixth residue in the Ca^{2+} binding loop is a common characteristic among all EF-hand motifs in the holo state.[49] This difference in hydrogen bonding is not reflected in the ψ and ϕ backbone torsion angles of residue G134, and its measured ϕ value can be reproduced solely from the hydrogen bond differences. The differences in the torsion angles are more pronounced for the subsequent residues in loop IV, namely, Q135, V136, and N137, in agreement with their relatively high ϕ values (Figure S6f). The changes in these torsion angles are associated with differences in the interactions of the Q140 side-chain oxygen, which is hydrogen bonded to the backbone amide hydrogen atom of β-strand residue N137 in the apo-like state (Figure S7) but positioned to coordinate Ca^{2+} in the holo-like state and thereby unable to engage with N137. However, despite the fact that communication between residue Q140 and the short β-sheet is absent in the holo-like state, this state is able to adopt the open conformation. This finding suggests that cross talk between the Ca^{2+} binding sites through the mini β-sheet does not play a crucial role in the opening of the hydrophobic pocket upon Ca^{2+} binding. Moreover, in the apo-like state, the backbone oxygen of Q135 is not oriented properly to chelate Ca^{2+}, as opposed to the case in the holo-like state (Figure S6f). It has been proposed earlier that the backbone oxygen of Q135 does not coordinate Ca^{2+} in loop IV in the apo-like state.[19] While this interaction exists in our apo-like ensemble, it is significantly weaker than in the holo-like state (Figure S8). We note that the differences noted here between the apo-like and holo-like states of $(Ca^{2+})_2$-E140Q-TR_2C take place despite the fact that both loops III and IV are occupied by Ca^{2+}. Taken together, these differences in Ca^{2+} coordination and hydrogen bonding between the two subensembles suggest that dissociation of Ca^{2+} from loop IV might be gated by the conformational fluctuations of this loop.

Residues in loop III experience smaller differences in the hydrogen bonding network and torsion angles between the exchanging states relative to residues in loop IV. Similar to the case in loop IV, the side chain of the first residue in loop III, D93, is hydrogen bonded to the sixth residue of the same loop, G98, in all holo-like conformers, while this hydrogen bond is

DOI: 10.1021/acs.biochem.5b00961
Biochemistry 2016, 55, 19−28

absent in all apo-like conformers. This hydrogen bond induces changes in the ϕ and ψ torsion angles of only D93 and not G98 (Figure S6a,b). The conformational changes affecting D93 also involve the hydrogen bond that D93 forms with Y138 only in the apo-like state of $(Ca^{2+})_2$-E140Q-TR_2C, which is also present in the apo-WT-TR_2C PDB structures. Notably, these changes take place even though loop III is coordinating Ca^{2+}, suggesting that the conformational transition triggered by the interactions of the carboxyl of residue 140 with Ca^{2+} in loop IV is intimately connected with long-range effects on loop III, yet the backbone oxygen of Y99 equally well coordinates Ca^{2+} in loop III in both apo-like and holo-like states, similar to the PDB structures and unlike the equivalently positioned Q135 in loop IV. The side-chain χ_1 torsion angle of the neighboring residue I100 shows an average change of 24° between the apo- and holo-like states. However, this change is not as significant as the *trans* to *gauche* change between the PDB structures of apo- and holo-CaM, which might explain the lower accuracy of the RAM-derived ensemble in reproducing the relatively high ϕ value of I100.

Interestingly, the dihedral angle distribution in the loop connecting α-helices F and G of the apo-like state of $(Ca^{2+})_2$-E140Q-TR_2C is almost identical to that of apo-cCaM (Figure S6d). Moreover, the differences in the hydrogen bond network also reveal that the FG loop is stabilized in the holo-like state by two hydrogen bonds between the side chain of R106 and the backbone amide hydrogen of L116. These hydrogen bonds are also present in some holo structures of cCaM, but never in the apo structures (Table S1).

(iii) Differences in Ca^{2+} coordination by Q140 and hence in hydrogen bonding and torsion angles in loop IV further determine the accessibility to the ligand binding pocket. When Q140 does not chelate Ca^{2+} [in the apo-like state of $(Ca^{2+})_2$-E140Q-TR_2C], we found that the hydrophobic packing of α-helices E and H is retained as in apo structures of cCaM from the PDB (Figure 6a). In particular, the hydrophobic side chains

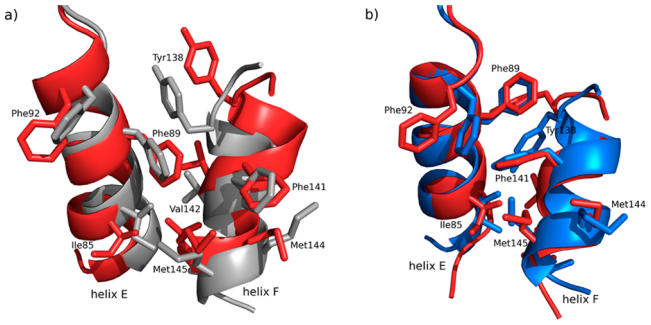

Figure 6. Hydrophobic packing between α-helices E and H in the apo-like and holo-like conformations of the $(Ca^{2+})_2$-E140Q-TR_2C ensemble. (a) Comparison of a representative apo-like structure (red) with the apo-WT-TR_2C structure (gray, PDB entry 1CMF). (b) Comparison of a representative holo-like structure (red) with the $(Ca^{2+})_2$-cCaM structure (blue, PDB entry 1CLL).

of F89, F92, and F141 do not engage in hydrophobic interactions and their side-chain orientations are almost identical to those observed in apo-WT-TR_2C. A slight difference in hydrophobic packing of α-helices E and H between apo-WT-TR_2C and the apo-like state of $(Ca^{2+})_2$-E140Q-TR_2C is observed for only Y138. The side chain of Y138 forms a hydrogen bond with D93 (loop III) in both apo-WT-TR_2C and the apo-like state of $(Ca^{2+})_2$-E140Q-TR_2C. The fact that loop III does not coordinate Ca^{2+} in apo-WT-TR_2C is the most likely reason for the differences in the rotameric states of Y138 in apo-WT-TR_2C and the apo-like state of $(Ca^{2+})_2$-E140Q-TR_2C.

On the other hand, when Q140 is positioned to chelate Ca^{2+}, the hydrophobic interactions between α-helices E and H are highly similar to those in the holo form of cCaM (Figure 6b). In particular, the coordination of Ca^{2+} by Q140 causes a rotation of α-helix H around its axis, which brings F141 into the proximity of F89 and F92. This movement of α-helix H and the rearrangement of the hydrophobic core between α-helices H and E cause a concomitant movement of α-helix E and the exposure of the protein hydrophobic core. The observed changes in the hydrophobic packing are identical to those of CaM upon Ca^{2+} binding.[9]

In summary, the presented analysis predicts that the holo-like state of $(Ca^{2+})_2$-E140Q-TR_2C is destabilized relative to $(Ca^{2+})_2$-cCaM, mainly because of the reduced coordination of Ca^{2+} in loop IV from a bidentate to a monodentate arrangement.[18,19] The formation of the two hydrogen bonds from the side chain of E140 is a crucial key for the structural change to occur upon Ca^{2+} binding. In earlier studies of CaM and other EF-hand proteins,[50−52] the role of the glutamic acid residue in position 12 of Ca^{2+} binding loops has been explored. In regulatory EF-hand proteins, this glutamic acid residue is generally believed to be important for the conformational changes to occur upon Ca^{2+} binding, which has been proposed for calbindin D9k in ref 53. Similarly, Sykes and co-workers[12] have identified Glu41 in skeletal TnC as a residue that "locks" the domain in the open form. In analogy, this study has emphasized the critical importance of E140 in wild-type cCaM, and its site-specific mutation has far-reaching effects on the structure of TR_2C, which are predicted with atomistic detail here. The mode of Ca^{2+} coordination in loop IV is intimately related to the backbone dihedral angles and hydrogen bonding patterns within both Ca^{2+} binding loops and leads to exposure of the target binding site through hydrophobic interactions between α-helices E and H, i.e., rotation of α-helix H driven by the reorientation of Q140.

The apo-like conformation of $(Ca^{2+})_2$-E140Q-TR_2C can be viewed as a model for the intermediate state on the pathway between the open, Ca^{2+}-loaded state and the closed, apo state. In this intermediate state, the loss of Ca^{2+} coordination by the carboxyl of residue 140 triggers a large-scale conformational change in the hydrophobic core and several local changes within loops III and IV that are characteristic of the apo state, thereby destabilizing the bound Ca^{2+} and serving to gate its dissociation from the binding sites. The allosteric process of closing and opening of $(Ca^{2+})_2$-E140Q-TR_2C that we have described thus provides unique insights into the atomistic determinants of CaM activation by calcium binding that go beyond those that can be achieved from analysis of the static structures of apo- and holo-CaM.

■ ASSOCIATED CONTENT

Supporting Information

The Supporting Information is available free of charge on the ACS Publications website at DOI: 10.1021/acs.biochem.5b00961.

Additional tables and figures (PDF)

DOI: 10.1021/acs.biochem.5b00961
Biochemistry 2016, 55, 19−28

AUTHOR INFORMATION

Corresponding Authors

*E-mail: mikael.akke@bpc.lu.se.

*E-mail: mv245@cam.ac.uk.

Funding

This work was supported by the Swedish Research Council (P.L., Dnr 2012-5136; M.A., Dnr 2010-4912), the Göran Gustafsson Foundation for Research in Natural Sciences and Medicine (M.A.), the Knut and Alice Wallenberg Foundation (M.A.), Biotechnology and Biological Sciences Research Council Grant BB/H013318/1 (P.K. and M.V.), a Federation of European Biochemical Societies Fellowship (C.C.), and a Marie Curie Intra European Fellowship (C.C.).

Notes

The authors declare no competing financial interest.

ACKNOWLEDGMENTS

We thank Alexandra Ahlner, Dan Adolfsson, and Sanela Smajilovic for sample preparation.

ABBREVIATIONS

CaM, calmodulin; TnC, skeletal troponin C; TR_1C, isolated fragment of the N-terminal domain of CaM; TR_2C, isolated fragment of the C-terminal domain of CaM; cCaM, C-terminal domain of full-length CaM; WT, wild type; NMR, nuclear magnetic resonance; NOE, nuclear Overhauser effect; RAM, replica-averaged metadynamics; HSQC, heteronuclear single-quantum coherence; NOESY, nuclear Overhauser effect spectroscopy; CV, collective variable.

REFERENCES

(1) Whitfield, J. (1991) *Calcium, cell cycles and cancer*, CRC Press, Boca Raton, FL.

(2) Xia, Z., and Storm, D. (2005) The role of calmodulin as a signal integrator for synaptic plasticity. *Nat. Rev. Neurosci. 6*, 267−276.

(3) da Silva, A. C., and Reinach, F. (1991) Calcium binding induces conformational changes in muscle regulatory proteins. *Trends Biochem. Sci. 16*, 53−57.

(4) Nelson, M. R., and Chazin, W. J. (1998) Structures of EF-hand Ca2+ binding proteins: diversity in the organization, packing and response to Ca2+ binding. *BioMetals 11*, 297−318.

(5) Akke, M., Forsén, S., and Chazin, W. (1995) Solution structure of (Cd2+)1-calbindin D9k reveals details of the stepwise structural changes along the Apo->(Ca2+)II1->(Ca2+)I,II2 binding pathway. *J. Mol. Biol. 252*, 102−121.

(6) Skelton, N., Kördel, J., Akke, M., Forsén, S., and Chazin, W. (1994) Signal transduction versus buffering activity in Ca2+ - binding proteins. *Nat. Struct. Biol. 1*, 239−245.

(7) Akke, M., Forsén, S., and Chazin, W. (1991) Molecular basis for co-operativity in Ca2+ binding to calbindin D9k: 1H nuclear magnetic resonance studies of (Cd2+)1-bovine calbindin D9k. *J. Mol. Biol. 220*, 173−189.

(8) Zhang, M., Tanaka, T., and Ikura, M. (1995) Calcium-induced conformational transition revealed by the solution structure of apo calmodulin. *Nat. Struct. Biol. 2*, 758−767.

(9) Chou, J., Li, S., Klee, C., and Bax, A. (2001) Solution structure of Ca2+−calmodulin reveals flexible hand-like properties of its domains. *Nat. Struct. Biol. 8*, 990−997.

(10) Kuboniwa, H., Tjandra, N., Grzesiek, S., Ren, H., Klee, C., and Bax, A. (1995) Solution structure of calcium-free calmodulin. *Nat. Struct. Biol. 2*, 768−776.

(11) Gagné, S., Tsuda, S., Li, M., Smillie, L., and Sykes, B. (1995) Structures of the troponin C regulatory domains in the apo and calcium-saturated states. *Nat. Struct. Biol. 2*, 784−789.

(12) Gagné, S., Li, M. X., and Sykes, B. (1997) Mechanism of direct coupling between binding and induced structural change in regulatory calcium binding proteins. *Biochemistry 36*, 4386−4392.

(13) Babu, S., Bugg, C., and Cook, W. (1988) Structure of calmodulin refined at 2.2 Å resolution. *J. Mol. Biol. 204*, 191−204.

(14) Chattopadhyaya, R., Meador, W., Means, A., and Quiocho, F. (1992) Calmodulin structure refined at 1.7 Å resolution. *J. Mol. Biol. 228*, 1177−1192.

(15) Evenas, J., Malmendal, A., Thulin, E., Carlstrom, G., and Forsen, S. (1998) Ca2+ Binding and Conformational Changes in a Calmodulin Domain. *Biochemistry 37*, 13744−13754.

(16) Finn, B., Evenäs, J., Drakenberg, T., Waltho, J., Thulin, E., and Forsén, S. (1995) Calcium-induced structural changes and domain autonomy in calmodulin. *Nat. Struct. Biol. 2*, 777−783.

(17) Evenas, J., Thulin, E., Malmendal, A., Forsen, S., and Carlstrom, G. (1997) NMR Studies of the E140Q Mutant of the Carboxy-Terminal Domain of Calmodulin Reveal Global Conformational Exchange in the Ca2+-Saturated State. *Biochemistry 36*, 3448−3457.

(18) Evenas, J., Forsen, S., Malmendal, A., and Akke, M. (1999) Backbone Dynamics and Energetics of a Calmodulin Domain Mutant Exchanging between Closed and Open Conformations. *J. Mol. Biol. 289*, 603−617.

(19) Evenas, J., Malmendal, A., and Akke, M. (2001) Dynamics of the Transition between Open and Closed Conformations in a Calmodulin C-Terminal Domain Mutant. *Structure 9*, 185−195.

(20) Linse, S., Helmersson, A., and Forsén, S. (1991) Calcium binding to calmodulin and its globular domains. *J. Biol. Chem. 265*, 8050−8054.

(21) Lundström, P., and Akke, M. (2005) Microsecond Protein Dynamics Measured by 13Calpha Rotating-Frame Spin Relaxation. *ChemBioChem 6*, 1685−1692.

(22) Lundstrom, P., and Akke, M. (2005) Off-resonance rotating-frame amide proton spin relaxation experiments measuring micro-second chemical exchange in proteins. *J. Biomol. NMR 32*, 163−173.

(23) Malmendal, A., Evenas, J., Forsen, S., and Akke, M. (1999) Structural Dynamics in the C-terminal Domain of Calmodulin at Low Calcium Levels. *J. Mol. Biol. 293*, 883−899.

(24) Camilloni, C., Cavalli, A., and Vendruscolo, M. (2013) Replica-averaged metadynamics. *J. Chem. Theory Comput. 9*, 5610−5617.

(25) Kukic, P., Camilloni, C., Cavalli, A., and Vendruscolo, M. (2014) Determination of the Individual Roles of the Linker Residues in the Interdomain Motions of Calmodulin Using NMR Chemical Shifts. *J. Mol. Biol. 426*, 1826−1838.

(26) Kukic, P., Alvin Leung, H. T., Bemporad, F., Aprile, F., Kumita, J., De Simone, A., Camilloni, C., and Vendruscolo, M. (2015) Structure and Dynamics of the Integrin LFA-1 I-Domain in the Inactive State Underlie its Inside-Out/Outside-In Signaling and Allosteric Mechanisms. *Structure 23*, 745−753.

(27) Camilloni, C., Cavalli, A., and Vendruscolo, M. (2013) Assessment of the Use of NMR Chemical Shifts as Replica-Averaged Structural Restraints in Molecular Dynamics Simulations to Characterize the Dynamics of Proteins. *J. Phys. Chem. B 117*, 1838−1843.

(28) Camilloni, C., Robustelli, P., De Simone, A., Cavalli, A., and Vendruscolo, M. (2012) Characterization of the Conformational Equilibrium between the Two Major Substates of RNase A Using NMR Chemical Shifts. *J. Am. Chem. Soc. 134*, 3968−3971.

(29) Muhandiram, R., and Kay, L. (1994) Gradient-Enhanced Triple-Resonance Three-Dimensional NMR Experiments with Improved Sensitivity. *J. Magn. Reson., Ser. B 103*, 203−216.

(30) Palmer, A. I., Cavanagh, J., Wright, P., and Rance, M. (1991) Sensitivity improvement in proton-detected two-dimensional heteronuclear correlation NMR spectroscopy. *J. Magn. Reson. 93*, 151−170.

(31) Hess, B., Kutzner, C., van der Spoel, D., and Lindahl, E. (2008) GROMACS 4: Algorithms for Highly Efficient, Load-Balanced, and Scalable Molecular Simulation. *J. Chem. Theory Comput. 4*, 435−447.

(32) Bonomi, M., Branduardi, D., Bussi, G., Camilloni, C., Provasi, D., Raiteri, P., Donadio, D., Marinelli, F., Pietrucci, F., Broglia, R., and Parrinello, M. (2009) PLUMED: a portable plugin for free energy

DOI: 10.1021/acs.biochem.5b00961
Biochemistry 2016, 55, 19−28

calculations with molecular dynamics. *Comput. Phys. Commun. 180*, 1961.
(33) Fu, B., Sahakyan, A. B., Camilloni, C., Tartaglia, G. G., Paci, E., Caflisch, A., Vendruscolo, M., and Cavalli, A. (2014) ALMOST: An all atom molecular simulation toolkit for protein structure determination. *J. Comput. Chem. 35*, 1101−1105.
(34) Lindorff-Larsen, K., Piana, S., Palmo, K., Maragakis, P., Klepeis, J., Dror, R., and Shaw, D. (2010) Improved side-chain torsion potentials for the Amber ff99SB protein force field. *Proteins: Struct., Funct., Genet. 78*, 1950−1958.
(35) Jorgensen, W., Chandrasekhar, J., Madura, J., Impey, R., and Klein, M. (1983) Comparison of simple potential functions for simulating liquid water. *J. Chem. Phys. 79*, 926.
(36) Essmann, U., Perera, L., Berkowitz, M., Darden, T., Lee, H., and Pedersen, L. (1995) A smooth particle mesh Ewald method. *J. Chem. Phys. 103*, 8577.
(37) Roux, B., and Weare, J. (2013) On the statistical equivalence of restrained-ensemble simulations with the maximum entropy method. *J. Chem. Phys. 138*, 084107.
(38) Cavalli, A., Camilloni, C., and Vendruscolo, M. (2013) Molecular dynamics simulations with replica-averaged structural restraints generate structural ensembles according to the maximum entropy principle. *J. Chem. Phys. 138*, 094112.
(39) Marinelli, F., Pietrucci, F., Laio, A., and Piana, S. (2009) A Kinetic Model of Trp-Cage Folding from Multiple Biased Molecular Dynamics Simulations. *PLoS Comput. Biol. 5*, e1000452.
(40) Biarnés, X., Pietrucci, F., Marinelli, F., and Laio, A. (2012) METAGUI. A VMD interface for analyzing metadynamics and molecular dynamics simulations. *Comput. Phys. Commun. 183*, 203−211.
(41) Humphrey, W., Dalke, A., and Schulten, K. (1996) VMD: Visual molecular dynamics. *J. Mol. Graphics 14*, 33−38.
(42) Bertini, I., Del Bianco, C., Gelis, I., Katsaros, N., Luchinat, C., Parigi, G., Peana, M., Provenzani, A., and Zoroddu, M. A. (2004) Experimentally exploring the conformational space sampled by domain reorientation in calmodulin. *Proc. Natl. Acad. Sci. U. S. A. 101*, 6841−6846.
(43) Camilloni, C., De Simone, A., Vranken, W., and Vendruscolo, M. (2012) Determination of Secondary Structure Populations in Disordered States of Proteins Using Nuclear Magnetic Resonance Chemical Shifts. *Biochemistry 51*, 2224−2231.
(44) Berman, H., Westbrook, J., Feng, Z., Gilliland, G., Bhat, T., Weissig, H., Shindyalov, I., and Bourne, P. (2000) The Protein Data Bank. *Nucleic Acids Res. 28*, 235−242.
(45) Rupp, B., Marshak, D., and Parkin, S. (1996) Crystallization and preliminary X-ray analysis of two new crystal forms of caimodulin. *Acta Crystallogr., Sect. D: Biol. Crystallogr. 52*, 411−413.
(46) Kursula, P. (2014) Crystallographic snapshots of initial steps in the collapse of the calmodulin central helix. *Acta Crystallogr., Sect. D: Biol. Crystallogr. 70*, 24−30.
(47) Kohlhoff, K. J., Robustelli, P., Cavalli, A., Salvatella, X., and Vendruscolo, M. (2009) Fast and Accurate Predictions of Protein NMR Chemical Shifts from Interatomic Distances. *J. Am. Chem. Soc. 131*, 13894−13895.
(48) Tjandra, N., Kuboniwa, H., Ren, H., and Bax, A. (1995) Rotational Dynamics of Calcium-Free Calmodulin Studied by 15N-NMR Relaxation Measurements. *Eur. J. Biochem. 230*, 1014−1024.
(49) Strynadka, N., and James, M. (1989) Crystal structures of the helix-loop-helix calcium-binding proteins. *Annu. Rev. Biochem. 58*, 951−998.
(50) Beckingham, K. (1991) Use of site-directed mutations in the individual Ca2(+)-binding sites of calmodulin to examine Ca2(+)-induced conformational changes. *J. Biol. Chem. 266*, 6027−6030.
(51) Maune, J., Klee, C., and Beckingham, K. (1992) Ca2+ binding and conformational change in two series of point mutations to the individual Ca(2+)-binding sites of calmodulin. *J. Biol. Chem. 267*, 5286−5295.
(52) Carlstrom, G., and Chazin, W. (1993) Two-dimensional 1H Nuclear Magnetic Resonance Studies of the Half-saturated (Ca^{2+})1 State of Calbindin D9k: Further Implications for the Molecular Basis of Cooperative Ca2+ binding. *J. Mol. Biol. 231*, 415.
(53) Wimberly, B., Thulin, E., and Chazin, W. (1995) Characterization of the N-terminal half-saturated state of calbindin D9k: NMR studies of the N56A mutant. *Protein Sci. 4*, 1045−1055.

DOI: 10.1021/acs.biochem.5b00961
Biochemistry 2016, 55, 19−28